Ann. Telecommunn. manuscript No.
(will be inserted by the editor)

Parametric Distributions of Connection Lengths for the Efficient Analysis of Fixed Access Network

Catherine Gloaguen · Florian Voss · Volker Schmidt

Received: date / Accepted: date

Abstract The access network displays an important particularity that the locations of the network components strongly depend on geometrical features such as road systems and a city's architecture. This paper deals with the distributions of point-to-point connection lengths that play a major role in current problems in the analysis and planning of networks. Using the mathematical framework of stochastic geometry to model both the road system and the locations of network nodes, we derive analytical formulas for distributions of connection lengths. These formulas depend explicitly on a few parameters that can be computed easily and fast avoiding time consuming reconstructions. We validate the approach by a comparison with actual network data and show its adaptability by considering several policies for nodes location and examples of use.

Keywords Stochastic Geometry · Palm Calculus · Telecommunication Networks · Communication Systems · Communication System Planning · Network Planning

1 Introduction

In order to meet user expectations for quality and security of their communications in a cost-effective way, the design of new architecture principles and concepts for future networks are currently being investigated by the telecommunication community. To cope with this rapid evolution and diversification of networks, it is necessary for the telecommunication operator to be able to select the best available solutions in terms of cost and efficiency. Accordingly, the scope of the methodology presented here is to offer easy to use, reliable and efficient tools to the network operator for the global analysis of huge networks that explicitly take into account the geometry of the territory while being able to describe various technologies and architectures.

Although perhaps not perceived by modern customers immersed in a world of mobility, the fixed part of the access network is nevertheless an important and omnipresent entity, which is based either on traditional (copper) or more recent (optical fibre) technologies. Due to its complexity in terms of a variety of equipment types, geographical settings and a history of successive amendments, this part of the network is for the network operator a major cost element as well as an important source of income. A characteristic feature of the fixed access network is its strong dependency on the geography and territory infrastructure, especially on the road system that is used as a natural guide for physical telecommunication lines. Key components of the quality of service or the technical feasibility of architecture solutions like connection lengths are thus very sensitive to the geometry of the network implantation and subject to regional and/or scale specificities. In order to study e.g. the impact of the morphology of the road system on the performance of a given network architecture, a natural way is to consider separately the geographical constraints, the placement of network components and their connections. Thus, we propose a geographically based analysis for fixed access networks accounting for regional specificities which is based on three distinct building blocks:

1. the geometrical support, i.e. the underlying road system,
2. the locations of network nodes along the roads,
3. the connection topology, i.e. the physical connection paths.

This work was supported by Orange Labs Research agreement 46143714

C. Gloaguen (corresponding author)
Orange Labs, 92794 Issy les Moulineaux Cedex 9, France
E-mail: catherine.gloaguen@orange-ftgroup.com

F. Voss · V. Schmidt
Institute of Stochastics, Ulm University, 89069 Ulm, Germany
E-mail: {florian.voss, volker.schmidt}@uni-ulm.de

This methodology allows us to deal with a variety of realistic situations. Pertinent quantities relevant to network performance evaluation or planning are usually estimated either by extraction from databases or by reconstruction. Each method has its own advantages and drawbacks. Databases are snapshots of network and offer in principle a true picture of reality. But they do not always describe all network parts, are not available for non–existent networks, do not contain equally reliable data and are huge and not easy to handle. Moreover, they are only descriptive by nature and thus do not give any straightforward interpretation of the actual network state. Exhaustive reconstruction of a given network implementation scenario provides precise and local information. However, network reconstructions are not suitable for application such as e.g. network planning. Due to large computation times the analysis based on reconstructions is restricted to a few cases that may not be representative for all possible network scenarios.

How to deal with these seemingly contradictory requirements: being able to provide rapid answers and estimation at global scale while being at the same time able to keep information on geographical features? A solution is to turn the intrinsic variability and the complexity of the whole network into an advantage. This is possible in the framework of stochastic modelling. The choice of random models and parameters allows to deal directly with the desired statistical information while taking into account the geographical features and offering an explicit relationship between the network and the morphology of the underlying territory.

The ”Stochastic Subscriber Line Model” (SSLM) [1] is a stochastic–geometric model for fixed access networks using the three building blocks introduced above. Since the first applications of spatial stochastic models to global network modelling [2,3], specific mathematical tools have been developed [4–6] in order describe the underlying road system as a whole or as a support for network nodes and connections. In [7] we showed that real road systems can be replaced by simulations of random models in order to estimate the distribution of point–to–point connection lengths. This representation of the road system by stochastic models defined by their type and parameters is the key point of the SSLM. Using a mixture of mathematical considerations and numerical simulations, it allows to derive parametric formulas that describe the relationship between the statistical distributions of the geometric network characteristics and the morphology of the road system. This is presented in [8] that validates the approach on the case of Paris access network.

This paper is an extended version of [8] and aims to emphasize that the SSLM is an open methodology both for its potential generalizations and applications. New policies for positioning of network nodes can easily be introduced in order to describe e.g. the network on the scale of the territory (see Section 4.3). It is also straightforward to describe and quantify the impact of network architecture and/or technology choices on geometry-dependent quantities that themselves play a major role in a number of current problems in the realm of analysis and planning of networks.

Section 2 briefly presents the access network and the SSLM principles. The mathematical aspects of spatial stochastic modelling are introduced in Sections 3 and 4. Section 5 validates the SSLM on the Paris example and demonstrates the adaptability of the model by taking into account geographical specifics and coping with some problems created by the introduction of optical fiber technology. Note that although other geometrical quantities could be considered, we focus on the analysis of connection lengths since they are highly sensitive to the geometry of the network and are therefore a good indicator to validate the proposed methodology.

2 Stochastic models for access networks

2.1 Technical overview of the access network

The purpose of a network is to allow connections and data transfer between customers. In this paper we mainly focus on the access network (or local loop) which is the lower part of the network, connecting a subscriber (the phone or the computer at home) by a physical link to its corresponding Wire Center Station (WCS) via intermediate network components. Connections between WCS nodes are assured by core network not considered here. The different types of access nodes play a concentration role, allowing the merging of low capacities cables to a single cable of higher capacity.

In a given area, the road system is built or planned in order to offer communication ways and/or access to the whole area. It is pre-existent to the telecommunication network: either in time or during the territory planning process. The underlying road system is itself a very complicated object. Its morphology depends on the scale of analysis, on the population density, the geographical constraints, the economic activity, etc. Since national roads and motorways are designed to connect major towns and small streets or dead ends are designed to reach every location inside the city, their overall shape and properties are very diverse (Fig. 1). Note that detailed road data is available in coordinate form, but similar to network databases, it is only descriptive and needs dedicated software to be handled.

Since both kinds of networks, i.e., road and telecommunication networks, have the goal to connect people, it is natural for the telecommunication network to use the road system that itself reaches the customers. Then access network nodes as well as connections strongly depend on the morphology of the road system. The cables run under pavements in trenches forming the civil engineering part of the whole telecommunication network. Thus, the fixed access network

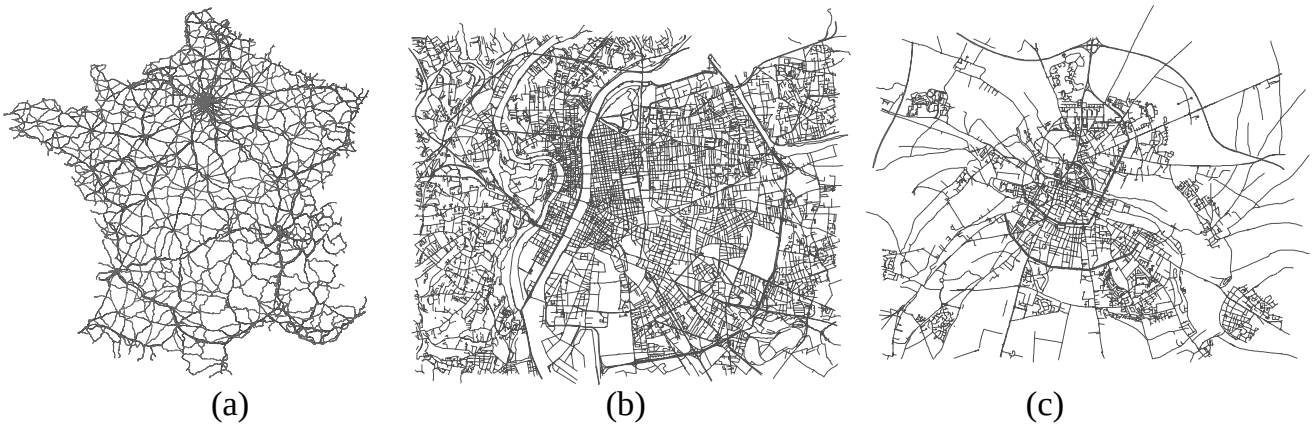

Fig. 1 The morphology of road systems depends on the scale of analysis. **a** Nationwide scale (width 950 km) motorways, national and some secondary roads in France. **b** Major city scale (width 12km) inner city and suburbs of Lyon. **c** Amiens (width 9 km) with transition to rural areas.

Fig. 2 The access network (cables in grey) merges in the urban road system.

can be considered as the place, where the telecommunication network merges into civil engineering (Fig. 2). Because the setup of a network with hierarchical architecture aims to decrease its costs with economy of scale induced by the merging of cables, a delicate trade-off has to be found between the costs of individual nodes and the costs of the cables depending on their capacities, while ensuring the technical feasibility of the solution: node capacities vs. demand and length of connections vs. path loss requirements. It is then of extreme importance to be able to take into account the spatial structure of the road system in the process of network analysis or planning.

2.2 Stochastic modelling principles

The power of stochastic modelling is to take advantage of the complexity of the system. It is particularly suited to our purpose which is to develop pertinent and reliable tools to analyse the network at global scale in order to compare various architectures and technologies.

Let us consider an example: knowing the exact connection length from a customer to its corresponding WCS may be of importance locally. However, it is difficult or even impossible to determine the connection lengths of all customers since the whole network has to be reconstructed. In particular, if future network designs have to be analysed, it is only possible to investigate a few possible scenarios due to limited computation time.

On the contrary, if one considers the whole set of customers and their connection distances to WCS, one observes a variability that can be interpreted in a statistical way as a distance distribution. This distribution contains important global information for the network operator like the percentage of customers that can be reached within a length threshold imposed by the technology.

However, at a macroscopic scale, global rules for connections or locations are more relevant than minute details annihilating each other. The main goal of stochastic modelling is to describe the spatial variability of each of the three blocks defined in Section 1 (geometrical support, locations of network nodes and connection topology) by random processes. Then the distributions of important network characteristics like connection lengths can be directly linked to parameters of the model which can be estimated from real data. Possible models in order to represent e.g. the geometrical support or the locations of network nodes are systems of randomly located points and lines which can be described in the framework of spatial stochastic processes. They are defined by a small number of parameters, but can reproduce geometrical and statistical features of real data and are therefore ideal components for the SSLM blocks.

2.2.1 Geometrical support

Objects (lines, points) are thrown in a random way to generate a paving of the plane (a ”tessellation”) whose edges can be used as a model for road systems. Several simple mod-

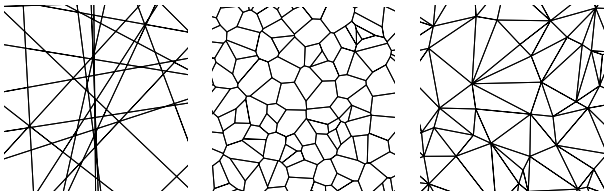

Fig. 3 Realizations of simple tessellations of the plane. **a** PLT. **b** PVT. **c** PDT .

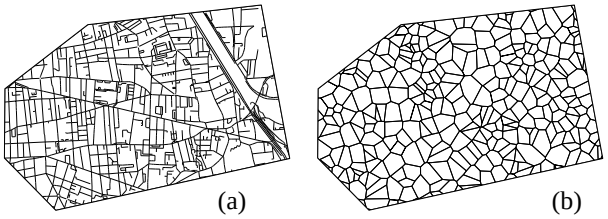

Fig. 4 **a** A real road system: 528 crossings, 324 quarters, 849 street segments and 97 km total street length. **b** The best statistically equivalent PVT with in average: 585 crossings, 293 quarters, 878 street segments and 82 km total street length.

els (Fig. 3) are available: tessellations constructed from lines (Poisson line tessellation (PLT)), from links between points (Poisson-Delaunay tessellation (PDT)) or from areas around points (Poisson-Voronoi tessellation (PVT)). Iterated tessellations obtained by combinations, and the possibility to include a fraction of empty areas, provide even more realistic models. Under the Poisson assumption of maximum randomness (the objects are located independently from each other and their number follows a Poissonian law), a simple homogeneous random tessellation is fully defined by a single parameter: its intensity. Then, mathematical developments can lead to exact analytical formulas relating statistical features of the tessellation to its type and intensity [9,10].

The vector $\mathscr{T} =$ (number of crossings, number of quarters, total length of streets, number of streets segments) averaged per unit area statistically describes the morphology of the road system. One can define the distance between a theoretical random model and the real road system by comparing the theoretical $\mathscr{T}$ to the vector of corresponding empirical quantities using, for example, the relative Euclidean norm. From the explicit dependence of $\mathscr{T} = \mathscr{T}(type, \gamma)$ on the type of model and its intensity γ, it is possible to choose the best model among a given set of candidates by minimizing the distance. This fitting procedure is described in [4]. Then the best model statistically reproduces the morphology of the real road system, but is described only by its type and intensity, see Fig. 4.

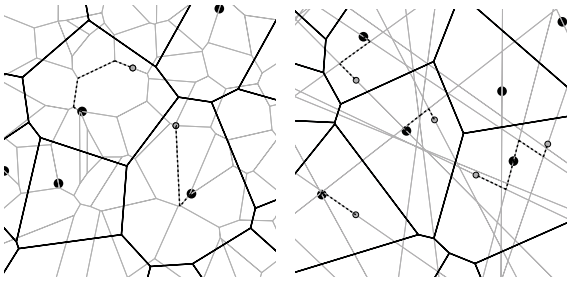

Fig. 5 HLC with their serving zones (black), some LLCs (grey with black boundary) and shortest paths (dashed) located along the edge set (grey). **a** Street model PVT. **b** Street model PLT.

2.2.2 Locations of network nodes

Since we are interested in point-to-point distances, it is sufficient to consider sub-networks involving two types of nodes: low-level components (LLC) and high-level components (HLC). Both types of nodes are randomly located along the road system. This reflects the variability of situations encountered in real networks.
In the simplest model, network nodes are positioned along the streets under the homogeneous Poisson assumption which will be used in Section 3 and most of Section 4. Then given a model for the street system, the intensity (the mean number of nodes per unit length of the street) is the only parameter required to fully determine the mathematical model for each node type. For rural networks this basic model has to be slightly adapted: the main nodes are located at the centre of villages, themselves located at crossroads (see Fig. 1 (a)). This location policy can be described by modelling the HLC set as a subset of road crossings (Fig. 10) and corresponding results are presented in Section 4.3.

2.2.3 Connection topology

We assume that LLC are logically connected to their nearest HLC, in the straight-line sense. This defines the serving zone of each HLC as the set of those points in the plane that are closest to it. Note that the serving zones are non-overlapping polygons and cover the whole plane, see Fig. 5. Furthermore, we assume that the physical connection from LLC to HLC is established as the shortest path following the streets. From analysis of available data, this appears to be a realistic assumption for the fixed access network. Thus, in the SSLM point-to-point distances are computed as lengths of shortest paths along the street system, linking two sets of nodes located randomly on the streets (Figs. 5 and 10). Using this framework we can derive analytical formulas for the distribution of distances between network nodes which explicitly depend on the topology of the underlying road system. More details on the mathematical methods are given below.

3 Mathematical methods and results

3.1 The Stochastic Subscriber Line Model

In this section we briefly describe the mathematical background of the stochastic network model which is considered in the present paper. The model is based on (marked) point processes and random tessellations, see [9,11,12] for details on these topics.

3.1.1 Random tessellations

A random tessellation T is a partition $\{\Xi_n\}$ of $\mathbb{R}^2$ into random (compact and convex) polygons Ξ_n which are locally finite. The polygons Ξ_n are called the cells of T. A random tessellation is called stationary if its distribution is invariant with respect to shifts of the origin o. We can identify T with its edge set $T^{(1)} = \bigcup \partial\Xi_n$, i.e., the boundaries of the cells of T. Now suppose that T is stationary. Then we define the intensity γ of T as $\gamma = \mathbb{E}\nu_1(T^{(1)} \cap [0,1]^2)$, i.e. the mean length of $T^{(1)}$ per unit area. In the following, we assume that T is either a PLT, a PVT or a PDT, see Fig. 3.

3.1.2 Typical shortest path length

For any T with intensity γ, we model the locations of HLC and LLC by linear Poisson processes $X_H = \{X_{H,n}\}$ and $X_L = \{X_{L,n}\}$ on the edges $T^{(1)}$ of T. Let λ_ℓ and λ'_ℓ denote the linear intensities of X_H and X_L, respectively. Then the planar intensities, i.e., the mean number of points per unit area, λ and λ' are given by $\lambda = \lambda_\ell\gamma$ and $\lambda' = \lambda'_\ell\gamma$. To each location $X_{H,n}$ of X_H we associate its Voronoi cell $\Xi_{H,n}$ with respect to X_H as its serving zone and define the segment systems $L_{H,n} = \Xi_{H,n} \cap T^{(1)}$ inside $\Xi_{H,n}$. All LLC are assumed to be connected to the HLC in whose serving zone they are located, i.e., $X_{L,n}$ is connected to $X_{H,j}$ if and only if $X_{L,n} \in L_{H,j} \subset \Xi_{H,j}$. In this way we can associate to each LLC a length C_n, namely the length of shortest path from $X_{L,n}$ to its closest HLC along $T^{(1)}$ (Fig. 5). Thus, we obtain the marked point process $X_C = \{(X_{L,n}, C_n)\}$. In the following we investigate the distribution of the typical shortest path length C^* which is defined as the typical mark of X_C. Formally, the distribution of C^* is defined as the Palm mark distribution ([11], Chapter 13.4) of X_C, but it can be regarded as the limit of empirical distributions of the shortest path lengths of all LLC in a sequence of unboundedly increasing sampling windows. Suppose e.g. that $W_n = [-n,n]^2$ and $h : \mathbb{R}^+ \longmapsto \mathbb{R}^+$ is some function, then

$$\mathbb{E}h(C^*) = \lim_{n\to\infty} \frac{1}{\#\{j : X_{L,j} \in W_n\}} \sum_{X_{L,j}\in W_n} h(C_j) \tag{1}$$

almost surely. Equation (1) motivates why we are interested in C^*, see also Section 2.2. Note that we can regard C^* as the shortest path length from the origin o to its nearest HLC under the condition that there is a LLC at o.

3.1.3 Typical serving zone

In the next section we show how the density f_{C^*} of C^* can be estimated based on simulations of the typical serving zone Ξ_H^* and the typical segment system L_H^* inside Ξ_H^*. The distribution of the typical serving zone can be regarded again as the limit of empirical distributions of the serving zones in a sequence of unboundedly increasing sampling windows or as the (conditional) distribution of the Voronoi cell at o given that there is a HLC located at o.

3.2 Density of shortest path length and its estimation

We now state a representation formula for the density f_{C^*} of C^* which depends only on the typical segment system L_H^* inside the typical serving zone Ξ_H^*. This formula is suitable to construct estimators for f_{C^*} based on i.i.d. samples of L_H^* which can be obtained from Monte Carlo simulation. If T is a PLT, PVT and PDT, respectively, then simulation algorithms for L_H^* are known, see [6, 13, 14].

3.2.1 Density of shortest path length

In the following, we derive a formula which allows us to compute the probability density of the typical shortest path length C^*. But we first state a formula which represents the quantity $\mathbb{E}h(C^*)$ in terms of L_H^*.

Lemma 1 *Let $c(y)$ denote the shortest path length from y to o. Then, for any measurable $h : \mathbb{R}^+ \longmapsto \mathbb{R}^+$, it holds that*

$$\mathbb{E}h(C^*) = \lambda_\ell \mathbb{E} \int_{L_H^*} h(c(y))\, \nu_1(dy). \tag{2}$$

Eq. (2) follows from Neveu's exchange formula for stationary marked point processes, see [15].

An important fact is that $\mathbb{E}h(C^*)$ does not depend on X_L and its linear intensity λ'_ℓ. We can rewrite (2) as

$$\mathbb{E}h(C^*) = \lambda_\ell \mathbb{E} \sum_{i=1}^{M} \int_{c(A_i)}^{c(B_i)} h(c(u))\, du, \tag{3}$$

where the segment system L_H^* is divided into line segments $S_1, \ldots, S_M$ with endpoints $A_1, B_1, \ldots, A_M, B_M$ such that $L_H^* = \bigcup_{i=1}^M S_i$ and $\nu_1(S_i \cap S_j) = 0$ for $i \neq j$, where $c(A_i) < c(B_i) = c(A_i) + \nu_1(S_i)$, see Fig. 6. Some segments of L_H^* are split in this way at so–called distance peaks. A point z on L_H^* is called distance peak if there are two different shortest paths with the same length from z to o.

With the notation introduced above we can derive a representation for the probability density f_{C^*} of C^* which can be used in order to estimate this density.

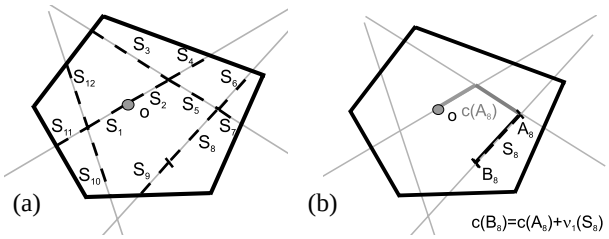

Fig. 6 L_H^* split into segments $S_1,\ldots,S_M$ (left) and single segment with distance peak B_8 (right)

Corollary 1 *The density f_{C^*} of the typical shortest path length C^* is given by $f_{C^*}(0) = 2\lambda_\ell$ and*

$$f_{C^*}(x) = \begin{cases} \lambda_\ell \, \mathbb{E} \sum_{i=1}^{M} \mathbb{1}_{[c(A_i),c(B_i))}(x) \text{ if } x \geq 0\,, \\ 0 \quad \text{otherwise}\,. \end{cases} \tag{4}$$

Formula (4) easily follows from (3), see [15].

3.2.2 Estimation of the density of shortest path length

In order to construct an estimator $\widehat{f}_{C^*}(x)$ for $f_{C^*}(x)$, we can use eq. (4). We are especially interested in the estimation of f_{C^*} from synthetic data obtained by simulations. The concept is then to simulate the typical serving zone Ξ_H^* together with the (typical) line segment system L_H^* in Ξ_H^*. Using Dijkstra's algorithm, the shortest path lengths $c(A_i)$ and $c(B_i)$ from all endpoints $A_1, B_1, \ldots, A_M, B_M$ to o can then be computed. This procedure is repeated n times, so we obtain for each $j = 1,\ldots,n$ the shortest path lengths $c(A_1^{(j)}), c(B_1^{(j)})$, $\ldots$, $c(A_{M_j}^{(j)}), c(B_{M_j}^{(j)})$ from the endpoints of the line segments. Finally, we can construct the estimator

$$\widehat{f}_{C^*}(x;n) = \lambda_\ell \, \frac{1}{n} \sum_{j=1}^{n} \sum_{i=1}^{M_j} \mathbb{1}_{[c(A_i^{(j)}),c(B_i^{(j)}))}(x)\,. \tag{5}$$

Note that $\widehat{f}_{C^*}(x;n)$ is a step function with respect to x. For each pair $c(A_i^{(j)}), c(B_i^{(j)})$ we add the value λ_ℓ/n for all $x \in [c(A_i^{(j)}), c(B_i^{(j)}))$ to $\widehat{f}_{C^*}(x;n)$. Thus, each additional segment with endpoints $A_i^{(j)}$ and $B_i^{(j)}$ yields new jumps at the points $c(A_i^{(j)})$ and $c(B_i^{(j)})$, see also Fig. 7.

The estimator $\widehat{f}_{C^*}$ possesses good statistical properties. For instance, $\widehat{f}_{C^*}(x;n)$ is unbiased for every $x \in [0,\infty)$ and the expectation $\mathbb{E}h(C^*)$ for some measurable function $h : [0,\infty) \mapsto [0,\infty)$ can be estimated unbiasedly by the estimator

$$\widehat{h(C^*)} = \int_{\mathbb{R}} h(x)\, \widehat{f}_{C^*}(x;n)\, dx\,.$$

Furthermore, it can be shown that the maximal deviation $\sup_{x\in[0,\infty)} |\widehat{f}_{C^*}(x;n) - f_{C^*}(x)|$ of $\widehat{f}_{C^*}(x;n)$ from the true density $f_{C^*}(x)$ converges to 0 with probability one as $n \to \infty$. For proofs of these results and further statistical properties of $\widehat{f}_{C^*}$ see [15].

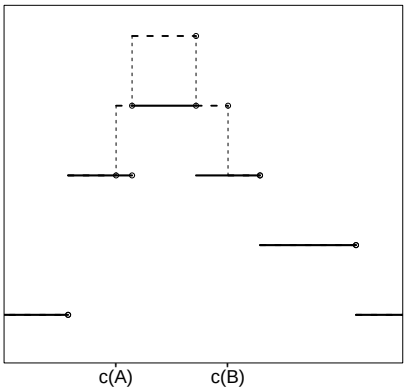

Fig. 7 $\widehat{f}_{C^*}$ is a step function. A segment with endpoints A and B with shortest path lengths $c(A)$ and $c(B)$ is added to $\widehat{f}_{C^*}$.

4 Parametric distance distributions

Now we present some numerical results obtained from a simulation study, where the road model $T^{(1)}$ is the edge set of a PDT, PLT and PVT, respectively, with intensity γ. Note that the considered models are scaling invariant, i.e., for all $\lambda_\ell, \gamma > 0$ with fixed quotient $\kappa = \gamma/\lambda_\ell$ we get the same model up to a scaling. Thus, for each κ, it is sufficient to compute numerical results for a single pair (γ, λ_ℓ) with $\gamma/\lambda_\ell = \kappa$. For further pairs $(\widetilde{\gamma}, \widetilde{\lambda}_\ell)$ with $\widetilde{\gamma}/\widetilde{\lambda}_\ell = \kappa$ the corresponding results can then be obtained by a suitable scaling, see [5]. Large κ yield a dense network inside the serving zones, whereas for small κ only a small number of segments intersect each serving zone.

To apply the model in a realistic setting, first an optimal tessellation T has to be fitted to the road system (Section 2.2.1). This step is fast and has to be done once. Each κ in then simply deduced from the wished intensity of nodes. Then the density f_{C^*} of the typical shortest path length C^* can be estimated by $\widehat{f}_{C^*}(x;n)$. But this estimation procedure for f_{C^*} is time-consuming especially for large κ and means, variances and quantiles have to be calculated numerically. Moreover, this requires the use of specialised simulation software.

For applications it would be of great benefit if the densities were given as parametric functions, with parameters only depending on κ and the type of the underlying road model T. Then, the distribution of C^* would be immediately available and time-consuming simulations and computations could be avoided. Therefore, the aim of this section is the construction of a whole library of parametric distance distributions for PDT, PLT and PVT as road models and a large range of κ. In the following we always consider the case that $\gamma = 1$ and values of κ between 1 and 2000 that cover realistic network scenarios.

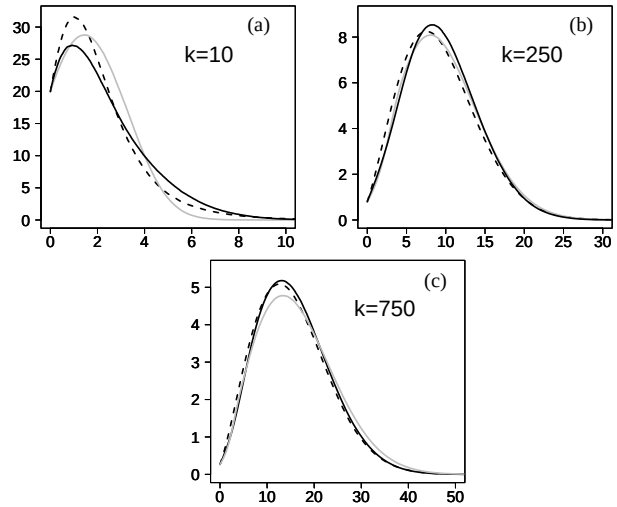

Fig. 8 Empirical density for linear Poisson processes of nodes with $\gamma = 1$ and PVT (grey), PDT (black), PLT (broken). Plot of 100*density as a function of length. **a** $\kappa = 10$. **b** $\kappa = 250$. **c** $\kappa = 750$.

4.1 Empirical densities estimated by simulations

We estimated the density f_{C^*} of the typical shortest path length C^* by simulating $n = 50000$ cells for values of κ between 1 and 2000 using the estimator $\widehat{f}_{C^*}(x;n)$ as explained in Section 3.2 for PDT, PLT and PVT. Some empirical densities obtained in this manner are displayed in Fig. 8. One can see that there is a clear difference between the shapes of the densities for small and large κ as well as for the different considered models. The differences between the densities for different models seem to decrease for increasing κ, but are still noticeable. In [16] it is shown that the typical shortest path length C^* converges in distribution to ξX as $\kappa \to \infty$, where $X \sim Wei(\lambda\pi, 2)$ and $\xi \geq 1$ is some constant depending on the tessellation model. For PLT we have $\xi = 1$, but $\xi > 1$ for PDT and PVT. So there will always remain some difference between the densities. Based on the estimated densities we computed means $\mathbb{E}C^*$, variances $\mathrm{Var}C^*$ and coefficients of variation $\mathrm{cv}C^* = 100\sqrt{\mathrm{Var}C^*}/\mathbb{E}C^*$. In Table 1 the means and cv's are displayed together with the corresponding results for the parametric densities fitted in Section 4.2 below to the estimated ones.

4.2 Fitting of parametric densities

In order to accurately represent empirical densities by analytical functions, we have to choose an appropriate parametric family of densities $\{f(x;\theta), \theta = (\theta_1, \ldots, \theta_k) \in \Theta\}$, where $\Theta \subset \mathbb{R}^k$ for some $k \geq 1$. Recall that C^* converges in distribution to the parametric limit distributions $Wei(\lambda\pi/\xi^2, 2)$ and $Exp(2\lambda_\ell)$ for $\kappa \to \infty$ and $\kappa \to 0$, respectively, where $\xi \geq 1$ is some constant depending on the road model T, see [16]. So it is reasonable to choose a parametric family which contains exponential and Weibull distributions as limiting cases. Furthermore, the parametric family $\{f(x;\theta), \theta = (\theta_1, \ldots, \theta_k) \in \Theta\}$ should possess the following properties.

1. The dimension k of $\theta = (\theta_1, \ldots, \theta_k)$ is small.
2. The parametric density $f(x;\theta)$ fits well for PDT, PLT and PVT and for a large range of κ, especially with respect to expectation and variance.
3. For each $\theta \in \Theta$, it holds that $f(0;\theta) = 2\lambda_\ell = 2/\kappa$.
4. The densities of $Wei(\alpha, 2), \alpha > 0$ and $Exp(\lambda), \lambda > 0$ are contained in $\{f(x;\theta), \theta \in \Theta\}$ as limiting cases.

It is not easy to choose a family of densities which fulfills all these conditions. The limit distributions $Wei(\lambda\pi/\xi^2, 2)$ and $Exp(2\lambda_\ell)$ are both special cases of a $Wei(\alpha,\beta)$–distribution. Since condition 3 can not be fulfilled in general by $Wei(\alpha,\beta)$–distributions, we shift their densities to the left and truncate them at zero such that condition 3 is fulfilled. In this way we get as one possible type of candidates the truncated Weibull distribution with density

$$f(x;\alpha,\beta) = C\Big(x+\big(\frac{2}{\alpha\beta\kappa}\big)^{\frac{1}{\beta-1}}\Big)^{\beta-1} e^{-\alpha\left(x+\left(\frac{2}{\alpha\beta\kappa}\right)^{\frac{1}{\beta-1}}\right)^{\beta}} \qquad (6)$$

for $x \geq 0$, where $C = \alpha\beta\exp((\alpha^{-1}(2/(\beta\kappa))^{\beta})^{1/(\beta-1)})$. This density has two parameters. Another candidate is a mixture $p\,f_1(x) + (1-p)\,f_2(x), p \in (0,1)$ of the densities f_1 of $Exp(\lambda)$ and f_2 of $Wei(\alpha,\beta), \beta > 1$. Again, condition 3 should be fulfilled, so we get

$$f(x;\alpha,\beta,\lambda) = 2e^{-\lambda x}/\kappa + (1-2/(\lambda\kappa))\alpha\beta x^{\beta-1}e^{-\alpha x^{\beta}}, \quad (7)$$

which has three parameters. We used Matlab to perform a weighted least squares fit of these parametric densities to the data $(\widehat{f}_{C^*}(x_1), \ldots, \widehat{f}_{C^*}(x_n))$ obtained from the empirical densities for a vector $(x_1, \ldots, x_n)$ with equidistant components. As weights we chose the reciprocals $1/\widehat{f}_{C^*}(x_1), \ldots, 1/\widehat{f}_{C^*}(x_n)$ in order to get a better fit at the tails of the densities. Then the optical fit of the densities is worse than without weighting, but the means and variances fit much better. Both regarded types of parametric densities fit optically quite well for all models and a large range of κ. Some estimated densities together with the fitted ones are displayed in Fig. 9 for truncated Weibull distributions. Similar results are obtained for mixtures of exponential and Weibull distributions. If we compare the expectations and variances of the fitted truncated Weibull distribution with the ones estimated from simulations, we can see that they match almost perfectly for all models and a large range of κ, see Table 1. Similarly, for mixtures of exponential and Weibull distributions the expectations fit quite good. However, the variances of the parametric densities differ clearly from the variances obtained from the estimated densities, although the optical fit between estimated and parametric densities is good. The reason might be

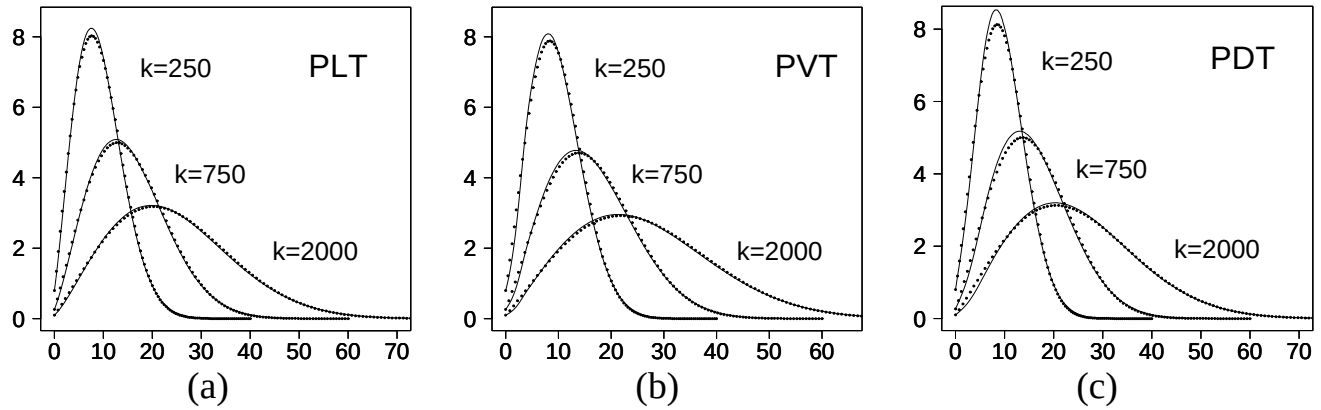

Fig. 9 Empirical density (line) with fitted truncated Weibull distribution (dots). Plot of 100*density as a function of length (unit=$1/\gamma$). **a** PLT. **b** PVT. **c** PDT.

Table 1 Mean and cv of C^* for empirical, fitted truncated Weibull and mixed exponential-Weibull distributions

PLT	$\mathbb{E}C^*$			cvC^*		
κ	emp.	trunc.	mix.	emp.	trunc.	mix.
5	1.510	1.450	1.511	95.4	93.8	120.8
10	2.181	2.111	2.175	83.9	78.0	103.6
50	4.505	4.469	4.450	60.2	59.7	70.8
500	12.69	12.71	12.72	51.8	51.4	57.5
1000	17.68	17.60	17.61	51.2	50.8	55.7
2000	24.24	24.30	24.31	51.1	50.7	54.3

PVT	$\mathbb{E}C^*$			cvC^*		
κ	emp.	trunc.	mix.	emp.	trunc.	mix.
5	1.397	1.391	1.387	73.5	73.7	83.7
10	2.054	2.055	2.059	63.5	63.3	80.3
50	4.552	4.511	4.540	52.0	52.9	69.6
500	13.46	13.49	13.51	50.9	50.6	61.2
1000	18.89	18.86	18.87	50.7	50.7	56.0
2000	26.34	26.34	26.36	51.0	50.9	54.7

PDT	$\mathbb{E}C^*$			cvC^*		
κ	emp.	trunc.	mix.	emp.	trunc.	mix.
5	1.744	1.723	1.712	92.5	91.8	80.5
10	2.367	2.378	2.373	76.6	76.1	77.9
50	4.780	4.757	4.768	54.1	54.6	69.0
500	13.05	13.06	13.08	49.3	49.1	57.7
1000	17.89	17.95	17.97	49.9	49.4	55.5
2000	24.72	24.64	24.85	50.4	50.8	54.0

that the exponential term in the mixture dominates the tails of this distribution yielding too large variances.

So the truncated Weibull distribution was chosen for the library. We calculated the parameters α and β for all three considered models and a large range of κ, where functions $\alpha(\kappa), \beta(\kappa)$ depending on κ were fitted to the estimated parameters for $\gamma = 1$. Thus, for all three model types, the distribution of C^* is now directly available up to a scaling via

$$f_{type}(x;\kappa) = f(x;\alpha_{type}(\kappa),\beta_{type}(\kappa)). \tag{8}$$

Probability theory and stochastic processes thus provide analytical formulas that are formally equivalent to statistical results computed on some reconstruction scheme, considering all the possibilities compatible with the geometrical setting. The hard work of listing and analyzing all those possibilities, with appropriate coefficients depending on their probability of occurrence is done by considering stochastic integrals, Palm probabilities, and the notion of the typical cell. Any reconstruction by hand, e.g. regarding the locations of nodes, would produce a configuration already considered.

4.3 Shortest path length for other point processes

The approach developed above in order to obtain parametric densities for the typical shortest path length C^* can also be used if the locations of HLC are modeled by point processes different from linear Poisson processes on the edge set $T^{(1)}$. For instance, X_H can be modeled by a thinned vertex set of T, where each vertex survives independently of the other vertices with some probability $p \in (0,1)$, see Fig. 10. If this model is considered, then Lemma 1 and Corollary 1 remain in principle true. However, the typical segment system L_H^* now corresponds to the point process X_H obtained from a thinning of the vertices of T and λ_ℓ is defined in this context by $\lambda_\ell = p\lambda^{(0)}/\gamma$. Here, $\lambda^{(0)}$ is the intensity of the point process of vertices of T. That means

$$f_{C^*}(x) = \begin{cases} \frac{p\lambda^{(0)}}{\gamma}\,\mathbb{E}\sum_{i=1}^{M} \mathbb{1}_{[c(A_i),c(B_i))}(x) \text{ if } x \geq 0, \\ 0 \quad \text{otherwise}, \end{cases} \tag{9}$$

and it holds that $f_{C^*}(0) = p\lambda^{(0)}/\gamma\,\mathbb{E}K^*$, where K^* is the number of edges emanating from the typical vertex. Thus, we can generate samples of L_H^* for thinnings of the vertices of T using simulation algorithms introduced in [15] and then compute the estimator $\widehat{f}_{C^*}$ for f_{C^*} introduced in

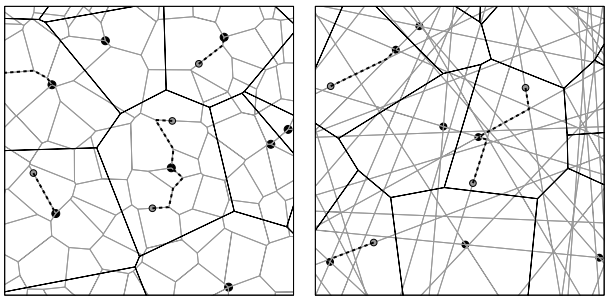

Fig. 10 HLC with their serving zones (black) and some LLCs (grey with black boundary) with shortest paths (dashed) along the edge set (grey). HLC are randomly chosen vertices from the underlying street model. **a** PVT. **b** PLT.

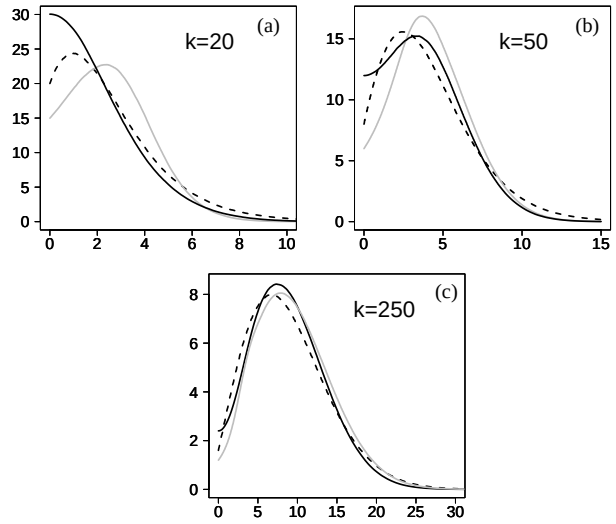

Fig. 11 Empirical density for thinned nodes with $\gamma = 1$ and PVT (grey), PDT (black), PLT (broken). Plot of 100*density as a function of length. **a** $\kappa = 20$. **b** $\kappa = 50$. **c** $\kappa = 250$.

eq. (5). In this way we obtain densities for the typical shortest path length of further network models which are different from the ones considered in the preceding section. For details we refer to [15]. Some densities estimated for thinnings are shown in Fig. 11, where the scaling factor κ is defined as $\kappa = \gamma/\lambda_\ell$ with $\lambda_\ell = p\lambda^{(0)}/\gamma$. Note that for given κ the survival probability p is given by $p = \gamma^2/(\lambda^{(0)}\kappa)$ with $\gamma^2/\lambda^{(0)} = \pi, 2$ and $(32/(3\pi))^2$ for PLT, PVT and PDT, respectively. As for linear Poisson processes, κ defines the structure of the model and hence the distribution of C^* up to a scaling. Note that especially for small values of κ there is a clear difference between the densities for linear Poisson processes and thinnings, compare Figs. 8 and 11.

Based on empirical densities for thinnings estimated by Monte Carlo simulations, we can again obtain parametric densities using the methodology developed above. This yields new classes of parametric distance distributions, see Fig. 12. Thus, the approach developed in this paper is very

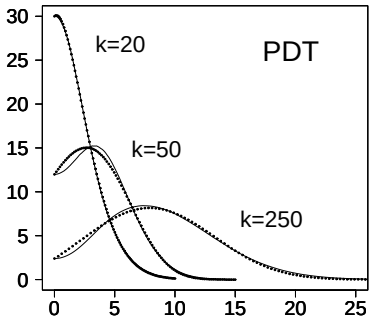

Fig. 12 Empirical density (line) with parametric distribution (dots) for thinned nodes on PDT. Plot of 100*density as a function of length (unit=$1/\gamma$)

flexible and can be easily generalized to further classes of models.

5 Application to real network analysis

In [7] we have shown that real road systems can be replaced by best fitted models as support for nodes by successfully comparing the histograms of shortest path connection lengths in the two settings of nodes: randomly located on the real road system or on the best fitted model. This validated the first building block of the SSLM. In the present paper, we go further by comparing real distance distributions obtained from databases for fixed access networks with the fitted parametric distributions that we developed above in the framework of the SSLM. In this Section we explain the methodology used in order to obtain real and parametric distance distributions. We then validate the model for the access network in Paris and in a smaller city i.e., we show that the parametric distributions are good approximations of real distance distributions. Finally, we discuss how the SSLM can be used to study the impact of new technologies or help at network planning.

5.1 Dealing with real data sets

The first step is to extract from the whole complexity of the database (being the result of a long history of modifications and changes) a synthetic view of the network not taking into account marginal situations. Again, the philosophy of stochastic models is to provide a global vision of a very complex situation that involves a huge number of equipments of various types, where the main features of the current network state have to be extracted from the amount of real data. The difficulty is to think ”stochastic geometry” while analyzing data so that they can be matched by the SSLM building blocks. Equipments or connections should not only be sorted according to their usual names or obvious functions, but by their geographical range and connection

Table 2 Comparison of characteristics of real data and fitted PVT model for Paris.

	real data	model
number of crossings	15462	17692
number of quarters	10613	8846
number of street segments	26056	26537
total length (km)	2146	1931
required input	database	2 parameters

principles. Let us briefly review these steps that have been done for the area of Paris.

5.1.1 Geometrical support and node location

In this paper, we shall consider only three simple tessellation models (PVT, PDT, PLT) that provide a sufficiently good description of the road system. In dense areas inside cities, dead ends only represent a small percentage of the total length of roads and can be ignored. Moreover the characteristics of the road system can be assumed to be homogeneous in the whole area of Paris. The fitting procedure applied to the road data, restricted to a possible choice from these simple tessellations, proposes a PVT model of intensity $\gamma = 18\ \mathrm{km}^{-1}$. The theoretical values of the relevant four characteristics of the fitted PVT model are very close to the measured ones as shown in Table 2.

All the network equipments referred in the databases to a common address are considered as geographical sites for node equipments located along the streets.

5.1.2 Structure in sub-networks

Data analysis shows that the total area A covered by the network can be divided into a set of non-overlapping zones on which distinct two-levels sub-networks are deployed. Each of these (large scale) zones contains only one highest WCS node. This division process of the total area A is repeated a second and a third time, yielding disjoint two-level sub-networks which are deployed at middle scale and lower scale zones, respectively. The zones arising at each of these three steps are non-overlapping and their union covers A. Some variability in shape and size can be observed, but the ranges of their average areas are well distinct.

This structure can be visualized by plotting the locations of the nodes using their geographical coordinates, where it must be kept in mind that the "frontiers" of the zones become more and more fuzzy from steps 1 to 3. Still, it remains possible to assume that the LLC considered at each step are logically connected to their closest HLC in flybird sense. Apart from A and the road-system characteristics, the only parameter required to describe a typical serving zone at a given step i is the number of HLC n_i from which the parameter κ_i can be computed; $i = 1, 2, 3$.

5.1.3 Histograms of connection lengths

Histograms of connection lengths are recovered from databases with respect to the above division into sub–networks. They concern the overall lengths of the telecommunication lines from any LLC to its respective HLC, but no information is available about their real physical path. The SSLM model proposes a global analysis in the most simple (idealized) setting that is compatible with the conclusion inferred from the analysis of databases: homogeneous random street system which captures the most important structural properties of the real street system, homogeneous random Poisson repartition of nodes along the streets, logical connection to the closest HLC in straight-line sense, physical connection as shortest path along the street system. All the geometrical objects are idealized points or line segments, whereas real cables possess physical constraints such as a minimum curvature radius as well as necessary cable-joining in chambers. Then the theoretical prediction for connection lengths from SSLM should naturally be lower than the observed ones.

5.2 Validation of the model for Paris

In order to describe the global statistical behavior of point-to-point connection lengths in the real access network of Paris, structured in three distinct two-level sub-networks, the SSLM only requires the knowledge of six global parameters:

- the size $|A|$ of network area A, the type of the road system inside A and its intensity (type=PVT,$\gamma = 18\ \mathrm{km}^{-1}$),
- the numbers n_1, n_2 and n_3 of higher-level nodes for each sub-network, where for steps 2 and 3, a HLC node may be part of the set of corresponding LLC nodes.

From the above values we directly deduce the parameters κ_1, κ_2 and κ_3 for the distance distributions. In all three examples considered below, the same family of parametric functions was used in eq. (8). The whole model is proposed under the form of an Excel sheet with functions encoded in Visual Basic, thus giving an instantaneous answer and also avoiding the need of specialized computing languages not easily accessible for managers.

Note that a few features of the real network were not mentioned above in order to simplify the presentation. Nevertheless, the figures presented here integrate all the reality of the network including some connections that arise in a non-purely hierarchical architecture as well as exclusion areas. This does not change the number of required parameters and analytical formulas, but only asks for the right combination of length distributions.

At step 1 the typical serving zone is relatively large compared to the scale of the road system since it contains in the average up to 200 quarters. This corresponds to a large value

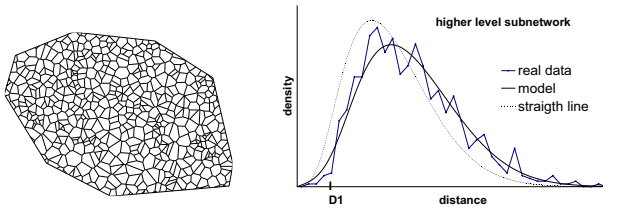

(a) (b)

Fig. 13 **a** Typical serving zone of the large scale sub-network $\kappa_1 = 1000$. **b** Parametric densities of connection lengths compared with histogram of real data, showing that the assumption of physical connections as straight-line shortest paths is incorrect.

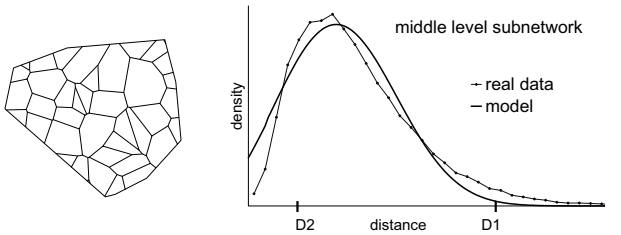

(a) (b)

Fig. 14 **a** Typical serving zone of the middle scale sub-network $\kappa_2 = 35$. **b** Rescaled parametric density of connection lengths compared with histogram of real data.

of $\kappa_1 \simeq 1000$ as illustrated in Fig. 13.a. The theoretical probability density fits extremely well with the histogram computed from real network data (see Fig. 13.b), in shape as well as length scale. Here D_1 denotes a reference distance to enable comparisons between results at different scales.

The typical serving zone at step 2 is much smaller since it contains approximately 10 quarters in the average, where $\kappa_2 \simeq 35$ (see Fig. 14.a). Note that the results obtained at this scale are based on connection lengths between various types of lower-level nodes which are all connected to the same type of HLC. In this case, the SSLM underestimates the average connection length by a factor $c = 1.15$. Thus, the theoretical distance density f has been rescaled in order to recover the measured average, i.e. $f(x) \to f(x/c)/c$, where it is assumed that the underestimation is due to an effect proportional to the distance. Model and real data are still close (see Fig. 14.b), whereas the distance scale (with unit distance D_2) is very different from the previous one (given by D_1).

Finally, the typical serving zone at step 3 is comparable in size with the area covered by a group of buildings. It contains only a few street segments and $\kappa_3 \simeq 4$ (see Fig. 15.a). The average connection length obtained from the SSLM underestimates the measured one by some value $l > 0$. This can be explained by the fact that real connection lengths include a part that goes from the building to the end customer not taken into account by the SSLM. Since this distance simply adds to the predicted length, the parametric density f has been shifted in order to recover the measured average, i.e.

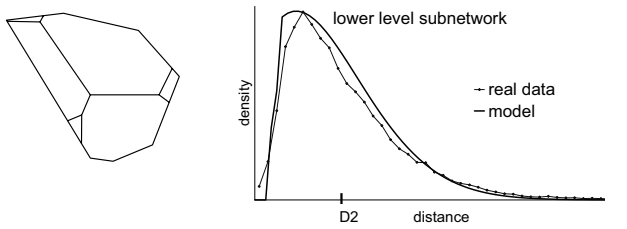

(a) (b)

Fig. 15 **a** Typical serving zone of the lower-scale sub-network $\kappa_3 = 4$. **b** Shifted parametric density of connection lengths compared with histogram of real data.

$f(x) \to f(x-l)$ for $x > l$. This leads to a very good fit between model and real data (see Fig. 15.c). Note that l thus determined from the comparison of model and real data is compatible with the value currently admitted in the network community. Again, the distance scale is rather different from the previous ones (given by D_1 and D_2, respectively).

We also remark that Fig. 13 illustrates the necessity to take into account the underlying road system. The theoretical distance distribution computed under the assumption that the physical connections are straight lines (dashed graph) does not fit to the histogram for real data and clearly underestimates the real average connection length. Classical studies introduce an estimated correction factor for the average length, but the SSLM explicitly relates it to the geometry of the underlying road system. Note that single WCS sub-networks have also been satisfactory addressed by the SSLM provided that one deals with a sufficiently large or diversified set of connections.

5.3 Analysis of smaller cities

The road system of Paris can be considered as homogeneous in the whole area of the city and thus the SSLM can be applied. On the contrary, smaller cities generally display a spatial variability of their road systems which is not homogeneous (Fig. 16.a). They can be divided into a few homogeneous parts that reflect their inner structure (city centers, suburbs, etc.). These parts can be modelled by a simple tessellation and its intensity. But a formal model of an access network that covers the whole city area should use mathematical methods which incorporate spatial inhomogeneity. However, the organization of the network in two-level subnetworks allows to propose a simpler approach by applying specifically the SSLM to each part of the city.

In the lower and middle scale sub–networks, the number of HLC is in general huge and thus the serving zones are small. Therefore, the part of the road system and the network inside the area of influence of each HLC can be regarded as (locally) homogeneous which allows to apply the SSLM. On the other hand, the network has a function of aggregation

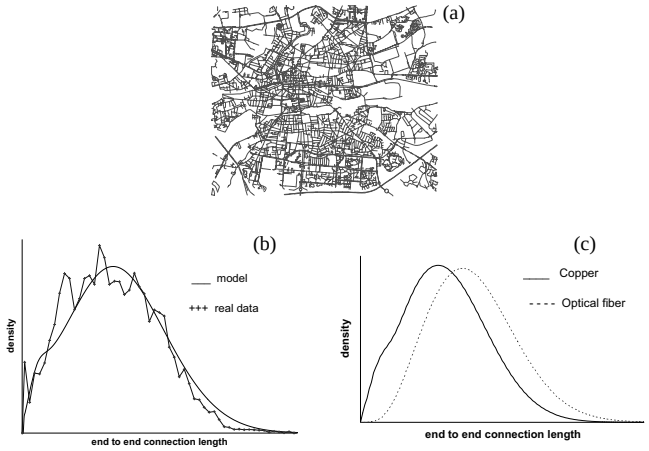

Fig. 16 **a** Road system in a middle sized French city. **b** Distribution of connection lengths from the customer to the higher level node of a 3 levels access network using copper technology deployed on the city area. **c** Impact of architecture, engineering rules and technology on the distribution of end–to–end connection lengths on the city area.

which results in a homogeneous distribution of the HLC of the large scale sub–network. We can then consider e.g. the main roads of the city as a homogeneous road system and, in this way, apply the SSLM also to the large scale sub–network.

For each part of the city, the distribution of the connection lengths from the customers to their corresponding highest level nodes is then obtained by convolving the length distributions of the relevant two-level sub–networks. Finally, the global distribution of the connection lengths for the whole network is estimated as the weighted average of the length distributions for each part of the city, where the weights depend on the number of customers in the respective part. This methodology provides sufficiently accurate results for length distributions to be used in global cost models (Fig. 16.b).

5.4 Some examples of the use of the SSLM

Given the parameters of the optimal road model in a given geographical area, the SSLM methodology allows us to analyse performance characteristics of any network deployed in this area. Due to the analytical formulas for lengths distributions developed in this paper, the computational time to analyse possible network scenarios (defined by its architecture, technology, number of nodes) does not depend on the size of the considered network and is almost zero.

The price to pay is the conceptual work needed to describe the desired scenario in terms of the SSLM building blocks (see Section 5.1). Architectures differ by the number and organization of the two-level sub-networks that share the area. Technology is taken into account by providing specific parameters to each type of nodes and connexions. For example optical lines are subject to losses due to coupling devices and specific attenuation proportional to their length; optical nodes are characterised by the maximum number of optical fibres they can manage. It remains to provide the number of nodes in order to estimate the parameters κ_i. Then a large number of scenarios can be efficiently investigated for the purpose at hand, ensuring that every conclusion takes into account all possible spatial configurations of nodes locations.

We choose two examples of current problems in the analysis of telecommunication networks to illustrate the adaptability of the SSLM. . The first example is the analysis of the impact of architecture and technology on the distribution of end–to–end connection lengths. It seems natural that connection lengths will differ for different scenarios, but how can we calculate this difference? On the same partitioning of the city as in Section 5.3, we described an optical network in the framework of the SSLM, i.e.we choose a specific architecture and deduce the number of optical nodes from population density and type of lodging, following requirements specific to optical equipments. Fig. 16.c displays the difference between the distribution of connection lengths for the actual copper network and for a possible (theoretical) optical network. Note that a full reconstruction is computationally impossible even in the case of this small city. This optical architecture can thereafter be used straightforwardly to analyse any other city for which road model, population and lodging type are known.

The second example concerns the planning of optical networks. Since the network architecture and the length (expressed in kilometres) distribution of lines are fully described by the SSLM, it is a simple matter to derive the probability density for the optical gain of the lines (expressed in decibels). The problem is to define which scenarios ensure that a given percentage of the lines (say 85 %) have total losses less than a fixed threshold. This offers a solution to the eligibility problem, i.e., to estimate the fraction of customers that can benefit of a new technology. To obtain Fig. 17, we considered the same optical architecture and city than above, two technology choices and varied the number of higher network nodes.

6 Conclusions and Outlook

The road system is the physical support that embeds the network nodes and connection cables of the fixed access network. Its geometrical characteristics have thus a strong impact on the overall characteristics and performance of the network. This paper shows that the SSLM, based on methods from stochastic geometry, is an excellent model to analyse huge access networks since it explicitly describes the morphology of the underlying road system in the expression

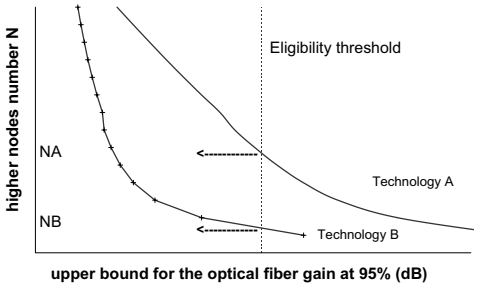

Fig. 17 The SSLM applied to planning. Choice of the number of nodes depending on the technologies under the constraint of eligibility threshold.

of geometrical network characteristics. Parametric distributions for connection lengths are derived and are successfully compared to distance distributions estimated from data of real access as in the very complex Paris network. The range of the model is far from being limited to this particular case. By construction, the SSLM consists of the components: geometrical support, locations of network nodes and connection topology. It is a toolbox that offers the possibility to address a wide range of potential applications by suitable combination of specific models for each component.

The simplest variation concerns the values of the entry parameters and/or the imbrications of the sub networks in the network description. For example, the results displayed in Fig. 16(b) for a small city are obtained by simply using the right parameters for their road systems. The impact of any new technology associated with an architecture for which no data are available can also be easily analysed as shown in Fig. 16(c). Further additions can be provided to the SSLM, like new policies for locating the nodes or modeling the road systems. The adaptation of the SSLM to regional scales is a current research topic for which automatized segmentation of road systems and new or more accurate road models are needed. For instance, in [17] we extend simulation procedures for the typical Voronoi cell of linear Poisson processes on simple tessellations to linear Poisson processes on iterated tessellations from which analytical formulas for distance distributions can be obtained. In this context, the thinning model for location of nodes introduced in Section 4.3 will be useful, since at this scale it is more realistic to assume that the higher level nodes are located in the centers of towns, i.e. in a subset of the crossings of the road system.

What is done of the SSLM output also offers a lot of possibilities. As mentioned above, we focused on the distribution of connection lengths because this quantity can be used for planning purpose. Since SSLM is fast, it can produce charts such as Fig. 17 without any computational time and help the operator to decide which possible scenarios should be investigated by detailed optimization procedures before their implementation. Other outputs such as distributions of degrees of nodes or areas of influence are simple to derive and can be part of realistic macroscopic cost functions, with explicit regional dependencies. A very important extension of the SSLM would be the description of random cabling trees (point–to–multipoint connections) for which the impact of the underlying road system cannot be neglected since it is impossible to build trees from straight-line connections that never share a common path. In addition, the morphology of the road system, especially the number of streets incoming in crossings, greatly influences the capacities of the cables to be installed.

References

1. Gloaguen C, Coupé P, Maier R, Schmidt V (2002) Stochastic modelling of urban access networks. In: Proc. 10th Internat. Telecommun. Network Strategy Planning Symp. VDE, Berlin, pp. 99–104.
2. Baccelli F, Klein M, Lebourges M, Zuyev S (1996) Géométrie aléatoire et architecture de réseaux. Annal Telecommun 51: 158–179
3. Baccelli F, Zuyev S (1996) Poisson-Voronoï spanning trees with applications to the optimization of communication networks. Oper Res 47: 619–631
4. Gloaguen C, Fleischer F, Schmidt H, Schmidt V (2006) Fitting of stochastic telecommunication network models, via distance measures and Monte-Carlo tests, Telecommun Syst 31:353–377
5. Gloaguen C, Fleischer F, Schmidt H, Schmidt V (2010) Analysis of shortest paths and subscriber line lengths in telecommunication access networks, Netw Spat Econ 10:15-47
6. Voss F, Gloaguen C, Fleischer F, Schmidt V (2009) Distributional properties of Euclidean distances in wireless networks involving road systems. IEEE JSAC 27(6):1047-1055
7. Gloaguen C, Schmidt H, Thiedmann R, Lanquetin JP, Schmidt V (2007) Comparison of network trees in deterministic and random settings using different connection rules. In: Proc. 3rd Workshop on Spatial Stochastic Models for Wireless Networks (SpaSWiN), Limassol
8. Gloaguen C, Voss F, Schmidt V (2009) Parametric distance distributions for fixed access network analysis and planning. In: Proc. 21st International Teletraffic Congress (ITC 21), Paris
9. Stoyan D, Kendall WS, Mecke J (1995) Stochastic Geometry and its Applications. John Wiley & Sons, Chichester
10. Maier R, Schmidt V (2003) Stationary iterated random tessellations. Adv Appl Prob (SGSA) 35:337-353
11. Daley D, Vere-Jones D (2008) An Introduction to the Theory of Point Processes (II). Springer, New York
12. Schneider R, Weil W (2008) Stochastic and Integral Geometry. Springer, Berlin
13. Fleischer F, Gloaguen C, Schmidt V, Voss F (2009) Simulation of the typical Poisson-Voronoï-Cox-Voronoi cell. JSCS 79(7):939-957
14. Gloaguen C, Fleischer F, Schmidt H, Schmidt V (2005) Simulation of typical Cox-Voronoï cells, with a special regard to implementation tests, Math Meth Oper Res 62(3):357–373
15. Voss F, Gloaguen C, Fleischer F, Schmidt V, Densities of shortest path lengths in spatial stochastic networks. Accepted for publication in Stochastic Models
16. Voss F, Gloaguen C, Schmidt V (2010) Scaling limits for shortest path lengths along the edges of stationary tessellations. Adv Appl Prob (in press)
17. Voss F, Gloaguen C, Schmidt V (2009) Palm calculus for stationary Cox processes on iterated random tessellations. In: Proc. 5th Workshop on Spatial Stochastic Models for Wireless Networks (SpaSWiN), Seoul.